Available online at www.sciencedirect.com
SCIENCE DIRECT
Journal of Catalysis 241 (2006) 83–95
JOURNAL OF CATALYSIS
www.elsevier.com/locate/jcat

On the "Active spacer and stabilizer" role of Zn in $Cu_{1-x}Zn_xFe_2O_4$ in the selective mono-N-methylation of aniline: XPS and catalysis study

Munusamy Vijayaraj, Chinnakonda S. Gopinath *

Catalysis Division, National Chemical Laboratory, Dr. Homi Bhabha Road, Pune 411 008, India

Received 30 January 2006; revised 7 April 2006; accepted 11 April 2006

Available online 30 May 2006

Abstract

A systematic catalytic methylation study on ferrospinel materials led to the selective production of N-methylaniline (NMA) with $Cu_{1-x}Zn_xFe_2O_4$. Aniline methylation was carried out on $Cu_{1-x}Zn_xFe_2O_4$ with a feed composition of CH_3OH:$PhNH_2$:H_2O = 3:1:1 at 513–633 K. NMA was formed selectively on all of the catalyst compositions, with trace amounts of secondary products under most of the conditions. $Cu_{0.5}Zn_{0.5}Fe_2O_4$ composition showed high catalytic activity and stability up to 100 h. Although the Cu^{2+} was responsible for methylation activity, Zn^{2+} enhanced the overall stability of the catalyst system. XPS investigations revealed that the degree of Cu^{2+} reduction decreased dramatically from $x = 0.05/0.25$ to $0.5/0.75$ on spent catalysts. TPR studies indicated that the reducibility of Cu^{2+} decreased from fully reducible at 523 K with Cu-rich compositions to partially reducible at 573 K on $x = 0.5$. Stable activity observed on $Cu_{0.5}Zn_{0.5}Fe_2O_4$ can be attributed to the highly heterogeneous distribution of metal ions. This heterogeneous distribution indicates an important role of zinc, likely as an "active spacer cum stabilizer" that hinders the reduction of active Cu^{2+} and contributes to prolonged activity.

Keywords: Ferrite; N-Methylation; Aniline; N-Methylaniline; XPS; TPR; Spacer; Stabilizer; Surface distribution

1. Introduction

N-Alkyl anilines are the basic raw materials for the production of dyes, synthetic rubber, explosives, herbicides, additives, antioxidants, and pharmaceuticals [1–6]. In general, the conventional route for producing any alkyl aromatics using mineral acids or Friedel–Craft-type catalysts [7,8] is economically cheap but highly non-environmental friendly due to the disposal problems of acid wastes and other problems, such as reactor corrosion. The liquid-phase aniline alkylation process carried out under pressure in the presence of various acids [7,8] or on K-exchanged zeolite-Y [9] is tedious, due to difficulties in separating the catalyst and product mixture.

Vapor-phase methylation of aniline over environmentally safe solid acid catalysts has been studied in the last few decades. Several types of solid catalysts based on oxides and supported oxides [10–12], zeolites [4,13–16] and microporous aluminophosphates [2,5,17,18] have been tested for aniline methylation, leading to N-methylaniline (NMA), N,N-dimethylaniline (DMA), and *o*-toludine (OT). Owing to the numerous uses of these anilines, the demand for the active and selective catalyst to a particular product has been grown over the period of time. Selective synthesis of NMA is difficult due to the presence of two chemically equivalent protons in amino group, which most often leads to dimethylation, and the process conditions cannot be changed beyond a limit for a high selectivity to NMA [12,19]. Ko et al. [12] studied the methylation of aniline with methanol at 698 K over alumina to give both NMA and DMA; the corresponding activation energies were 62.7 ± 2.1 and 48.3 ± 2.9 kJ mol^{-1}, respectively. It is obvious that NMA reacts faster than aniline and facilitates the consecutive methylation to DMA that leads to poor product selectivity or highly selective DMA production. Elangovan et al. [19] reported aniline methylation over AFI- and AEL-type molecular sieves at 623–673 K, where NMA, DMA, and N-methyl toluidines (NMT) were formed. The influence of different reaction parameters on the product distribution has also been analyzed. Rao et al. [20] tested aniline methy-

* Corresponding author. Fax: +91 20 2590 2633.
E-mail address: cs.gopinath@ncl.res.in (C.S. Gopinath).

0021-9517/$ – see front matter
doi:10.1016/j.jcat.2006.04.010

lation with DMC to compare the selectivity between NMA and DMA on zeolites such as EMT, faujasite, and alkaline loaded zeolite-β in the temperature range of 453–503 K and achieved 75% dimethylation selectivity. Bautista et al. [2,5,18] extensively studied the N-methylation of aniline over aluminum and chromium phosphates and observed a pseudo-first-order kinetic dependence with respect to aniline concentration. Their study of the effect of surface acidity on aniline alkylation by pyridine and 2,6-dimethyl pyridine adsorption experiments revealed that weak to moderate acid sites seem to be responsible for the reaction [2,5,18].

Our earlier characterization studies on alkylation of phenol and aniline on $Cu_{1-x}Co_xFe_2O_4$ [21–24] and $Cu_{1-x}Zn_xFe_2O_4$ [25,26] using XPS and in situ FTIR, respectively, led to an understanding of the electronic, structural, and mechanistic aspects of the alkylation reactions. Our earlier work on spinels at National Chemical Laboratory [21–27] revealed the potential catalysts for various alkylations. A thorough search for the selective catalytic production of N-monomethylation of aniline was carried out with $A_{0.5}A'_{0.5}Fe_2O_4$ systems, where A = Fe, Cu, Zn and A′ = Fe, Co, Ni, Cu, and Zn. Vapor-phase mono-N-methylation of aniline with methanol on $Cu_{1-x}Zn_xFe_2O_4$ is reported here. X-ray photoelectron spectroscopy (XPS), X-ray induced Auger electron spectroscopy (XAES), X-ray diffraction (XRD), and temperature-programmed reduction (TPR) investigations were carried out to evaluate the electronic and structural properties of the $Cu_{1-x}Zn_xFe_2O_4$ system and the interaction between the metal ions.

2. Experimental

2.1. Catalyst synthesis and characterization

Catalysts were prepared by adopting a low-temperature pH-controlled co-precipitation method, as reported previously [21–27]. The chemical compositions of calcined samples were determined by inductively coupled plasma spectrometry (ICPS) using a Perkin-Elmer PE 1000 device. XRD patterns of the powder samples were recorded using a Rigaku Geigerflex instrument using Cu-K_α radiation (1.5405 Å) with a Ni filter to verify the phase purity and obtain the unit cell parameter (a, Å) and crystallite size. The crystallite size of the samples was calculated using Scherrer's equation [21,28]. The BET surface area and the pore volume (V_p) of the catalysts were determined by N_2 adsorption–desorption at 77 K using a Quanta chrome NOVA-1200 adsorption unit. All of the above characterization results are given in Table 1. TPR experiments were carried out with a Micromeritic Autochem 2910 catalyst characterization system equipped with a thermal conductivity detector. Calcined catalysts were activated in Ar flow at 773 K for 1 h. After cooling to ambient temperature, the argon flow was replaced by a 5% H_2/Ar mixture. The catalysts were heated to 1073 K at a heating rate of 5 K/min. A flow rate of 30 mL/min was maintained throughout the experiments for all catalysts.

X-Ray photoelectron spectra were acquired on a VG Microtech Multilab ESCA 3000 spectrometer using a non-monochromatized Mg K_α X-ray source (1253.6 eV) on in situ scraped fresh catalyst pellets and powder samples of spent catalysts [21,29–31]. Selected spectra were recorded with an Al-K_α X-ray source (1486.6 eV) also to eliminate the overlap between different Auger and core levels. Base pressure in the analysis chamber was maintained in the range of $3–6 \times 10^{-10}$ Torr. The error in the reported BE values is ±0.1 eV.

2.2. Catalytic activity measurements

Vapor-phase methylation of aniline was carried out at atmospheric pressure in a fixed-bed, vertical-downflow glass reactor placed inside a double-zone furnace (Geomechanique, France). The 0.75-g sample of freshly calcined catalyst with 10 mesh particle size was charged each time in the center of the reactor in such a way that the catalyst was sandwiched between layers of inert porcelain beads. The upper portion of the reactor system served as a vaporizer cum preheater. The exact temperature of the catalyst bed was monitored with a K-type thermocouple placed at the center of the catalyst bed. The reactant mixture (methanol + aniline + water) was fed using a syringe pump (Braun, Germany) at a desired space velocity. Reaction products were collected from a condenser fixed below the reactor and analyzed using a gas chromatography (Agilent 19091J-413) with a HP-5.5% phenyl methyl siloxane capillary column equipped with a flame ionization detector and/or gas chromatography–mass spectroscopy (Shimadzu GC-17A equipped with a QP 5000 mass spectrometer).

3. Results

3.1. Effect of various metal ions toward N-methylation

Fig. 1 shows the aniline conversion and NMA yield on $A_{0.5}A'_{0.5}Fe_2O_4$ (A = Fe, Zn, Cu and A′ = Fe, Co, Ni, Cu, and Zn) at 573 K with a CH_3OH:$PhNH_2$ ratio of 3:1. NMA formed selectively on all of the systems; however, aniline conversion declined on all of the systems with TOS due to catalyst

Table 1
Chemical analysis, XRD parameters, and surface area of $Cu_{1-x}Zn_xFe_2O_4$

x	Metal concentration (wt%)			Crystallite size fresh (spent) (nm)	Lattice constant fresh (spent) a (Å)	S_{BET} fresh (spent) (m^2/g)
	Cu	Zn	Fe			
0.05	22.94	1.19	57.65	10.0 (23.4)	8.3459 (8.3723)	23.0 (16.0)
0.25	21.65	5.51	54.43	15.9 (19.5)	8.4090 (8.3946)	45.2 (34.0)
0.5	15.02	10.40	50.70	10.7 (12.1)	8.4052 (8.4133)	49.3 (41.0)
0.75	6.82	16.70	50.04	11.7 (19.5)	8.4150 (8.4153)	42.0 (22.0)
1	–	24.22	49.56	13.0 (16.0)	8.4180 (8.4117)	35.0 (28.0)

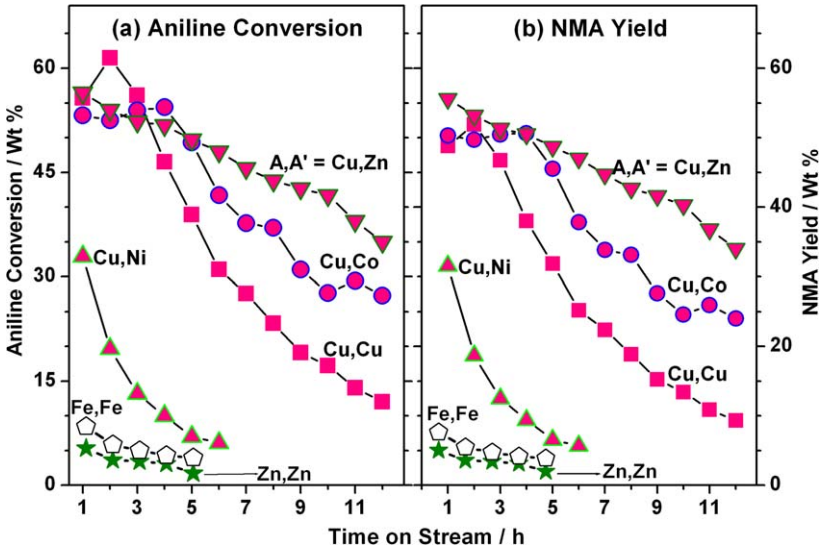

Fig. 1. Aniline conversion and N-methylaniline yield obtained on $A_{0.5}A'_{0.5}Fe_2O_4$ (A = Fe, Zn, Cu and A′ = Fe, Co, Ni, Cu and Zn) at 573 K with 3:1 ratio of CH_3OH:$PhNH_2$. Note a better initial catalytic activity was observed when Cu occupies the A-site in ferrites and the stability increases considerably when Zn also occupies the same site.

deactivation and/or coke deposition. The high initial aniline conversion to NMA associated with Cu-containing ferrospinel indicates that Cu was largely responsible for selective catalytic methylation activity. The addition of other metal ions to Cu, such as Co and Zn, improved the stability of the systems; however, addition of Ni decreased the activity. It is interesting to note that the $Cu_{0.5}Zn_{0.5}Fe_2O_4$ showed stable and better activity than the other systems; this indicates that Zn plays an important role in the stability of the system, even though negligible activity was found on $ZnFe_2O_4$. Individual oxides, including CuO, ZnO, CoO, Fe_2O_3, and CuO–ZnO, also demonstrated negligible or no activity toward aniline methylation (data not shown). A combination of Cu, Zn, and Fe in $Cu_{1-x}Zn_xFe_2O_4$ showed high and stable activity for aniline N-methylation, indicating the need for a suitable multicomponent system. For the foregoing reasons, the $Cu_{1-x}Zn_xFe_2O_4$ system was chosen for the detailed catalytic and characterization studies.

3.2. Catalyst characterization (XRD, chemical analysis, and surface area)

Table 1 presents the chemical compositions and structural and textural properties of $Cu_{1-x}Zn_xFe_2O_4$ system. ICPS results show the bulk metal ion concentration in weight percent. After reaction with CH_3OH:$PhNH_2$:H_2O (3:1:1) at 573 K for 8 h, all of the spent catalysts exhibited decreased surface area compared with fresh catalysts, due to carbon deposition. However, no significant decrease in surface area was observed for the $x = 0.5$ system. Fig. 2 shows the XRD reflection patterns of all of the calcined and spent catalysts. All of the fresh samples exhibited diffraction reflections attributed to the cubic spinel phase shown in Fig. 2; however, impurities such as CuO and Fe_2O_3 phases were also identified, as reported in JCPDS files. It is known that $CuFe_2O_4$ spinel formation cannot be completed at 773 K [21]; in fact, small amounts of Zn ($x = 0.05$) were added mainly to increase the spinel-phase purity and provide a Cu-rich system. Comparing our earlier XRD pattern of $CuFe_2O_4$ [21] and the present $Cu_{0.95}Zn_{0.05}Fe_2O_4$ showed that the impurities mostly, but not fully, disappeared, with a corresponding increase in spinel phase.

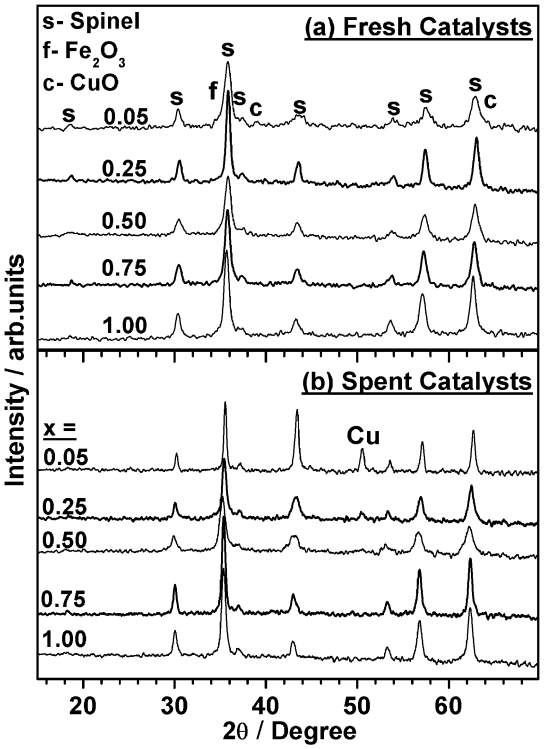

Fig. 2. X-Ray diffractogram of fresh and spent $Cu_{1-x}Zn_xFe_2O_4$ catalysts. XRD from spent catalysts are obtained after aniline methylation at 573 K for 8 h with 3:1:1 composition of methanol:aniline:water. Note the metallic Cu is observed only for $x = 0.05$ and 0.25.

The spent catalysts were examined in a similar fashion. Fig. 2b shows the XRD pattern, with a peak corresponding to Cu^0 observed for only the $x = 0.05$ and 0.25 compositions.

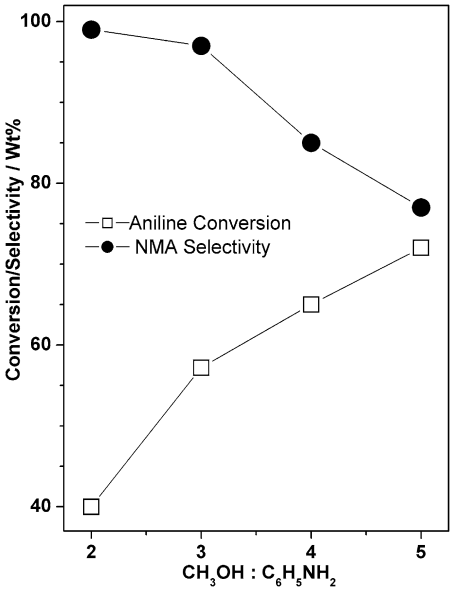

Fig. 3. Methanol:aniline:water feed composition (between 2:1:1 and 5:1:1) dependence of $PhNH_2$ conversion and NMA selectivity on $Cu_{0.5}Zn_{0.5}Fe_2O_4$ at 573 K and TOS = 8 h. 1:1 aniline:water ratio is maintained in all the feed compositions.

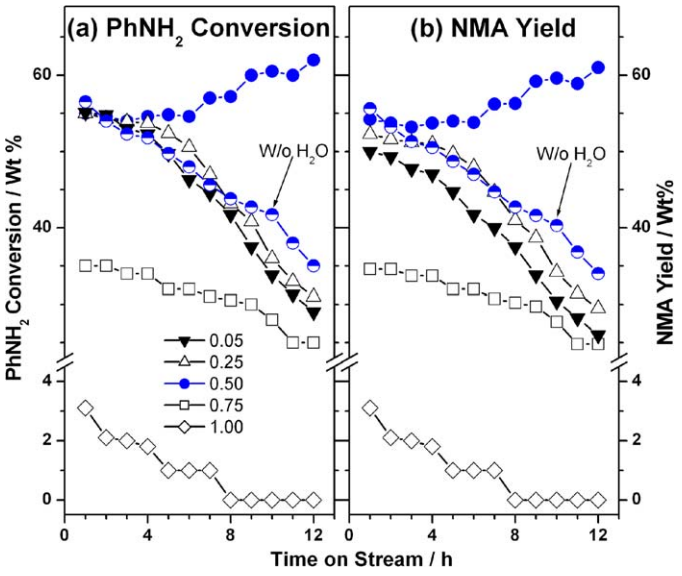

Fig. 4. TOS dependence of aniline conversion and NMA yield on $Cu_{1-x}Zn_xFe_2O_4$ at 573 K and WHSV = 3.58 h^{-1} with a feed composition of 3:1:1 of $MeOH:PhNH_2:H_2O$. Feed without water was also employed for $x = 0.5$ composition and denoted by half-filled circles.

This indicates the reductive reaction conditions after a time on stream (TOS) of 8 h. No Cu^0 is observed with other catalyst compositions. The increased crystallite size of spent catalysts, except for $x = 0.5$, hints to some sintering effect under the reaction conditions.

3.3. Catalytic conversion of aniline to N-methylaniline (NMA)

3.3.1. Effect of methanol to aniline molar ratio

The optimum composition of reactants was determined by carrying out aniline methylation using $CH_3OH:PhNH_2:H_2O$ molar ratios between 2:1:1 and 5:1:1 on $Cu_{0.5}Zn_{0.5}Fe_2O_4$ at 573 K (Fig. 3). It is to be noted that no water was added in the feed in the results shown in Fig. 1, and that the results shown in Figs. 3 and 4 are considerably different due to the addition of water. It is well known that adding water improves the stability of the catalytic system by avoiding coke deposition through the water–gas shift reaction. Aniline conversion increased gradually with increasing MeOH molar ratio up to 5; however, NMA selectivity decreased from 99 to 77%. This shows that a linear increase in aniline conversion (NMA selectivity) is directly (inversely) proportional to the amount of MeOH in the feed. Because the reaction was performed in vapor-phase conditions, some amount of MeOH was lost due to unavoidable side reactions, including steam reforming of methanol (SRM) and simple gasification. Hence an excess amount of MeOH is necessary, even though the reaction stoichiometry suggests a $CH_3OH:PhNH_2$ molar ratio of 1:1. Optimum feed composition was fixed as 3:1:1, at which a maximum aniline conversion with the desired NMA selectivity was observed. However, our previously reported in situ FTIR results [26] showed that the reaction stoichiometry was closely obeyed on the catalyst surface at 473 K during NMA formation.

3.3.2. Effect of $Cu_{1-x}Zn_xFe_2O_4$ catalyst composition

Fig. 4 shows the aniline conversion (a) and NMA yield (b) on $Cu_{1-x}Zn_xFe_2O_4$ ($x = 0.05$, 0.25, 0.5, 0.75, and 1) at $T = 573$ K, WHSV = 3.58 h^{-1}, and a 3:1:1 molar ratio of $CH_3OH:PhNH_2:H_2O$. Activity studies were carried out without water in the feed; a specific result on $x = 0.5$ is included to show the effect of adding water. Note that the samples with $x = 0.05$ and 0.25 showed initially high aniline conversions that rapidly decreased with increasing TOS. The sample with $x = 0.5$ showed stable activity, and indeed, a marginal increase in activity occurred at TOS > 6 h. The activity loss in the absence of water was due mainly to coke deposition. This was further confirmed by thermogravimetric analysis of deactivated samples in air. $ZnFe_2O_4$ showed negligible activity compared with other compositions, indicating a negligible role of direct methylation on Zn and Fe. Nevertheless, the catalyst stability associated with $x = 0.5$ under reaction conditions seemed to be enhanced, likely due to the presence of an optimum amount of Zn in it. The same effect was reflected in the extended activity measurement for 100 h (vide infra, Fig. 6).

3.3.3. Effect of reaction temperature and catalyst composition

Temperature-dependent catalytic activity measurements obtained at TOS = 8 h are shown in Fig. 5. It is clear that the maximum aniline conversion was at 573 K on all Cu-containing compositions with a volcano-type activity pattern with temperature and a maximum at $x = 0.5$. NMA selectivity remained >90% on all of the catalyst compositions; however, it decreased with increasing temperature. Between 543 and 633 K, $x = 0.5$ showed maximum aniline conversion with >93% NMA selectivity and stable activity, indicating that equal amounts of Cu and Zn are critical to the effective mono-N-methylation of aniline. A small amount of OT was formed along with DMA (data not shown) at high reaction temperatures ($\geqslant$ 603 K)

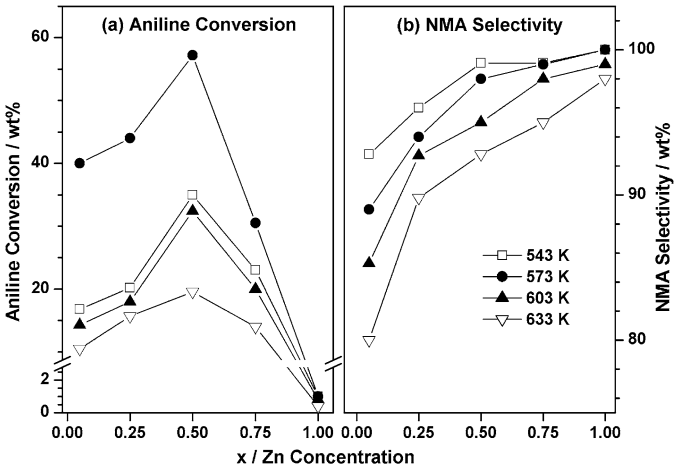

Fig. 5. $PhNH_2$ conversion and NMA selectivity dependence on reaction temperature and $Cu_{1-x}Zn_xFe_2O_4$ compositions at TOS = 8 h and WHSV = 3.58 h^{-1} with 3:1:1, CH_3OH:$PhNH_2$:H_2O.

on Cu-rich compositions. The maximum catalytic activity observed at 573 K was further confirmed by measuring the reaction first at 633 K and then at 573 K on $Cu_{0.5}Zn_{0.5}Fe_2O_4$. The above reaction carried out at 573 K in the second step showed 50% aniline conversion, compared with the 19% conversion seen at 633 K. However, a marginal decrease in aniline conversion in the second step (above) compared with the 54% conversion in the reaction carried out directly at 573 K (Fig. 4) hints at a slow change in catalyst surface properties at high temperature (633 K) due to a small amount of SRM and/or decomposition of MeOH.

3.3.4. *Effect of weight hour space velocity or contact time and TOS stability*

Fig. 6 shows the aniline conversion and NMA selectivity on $Cu_{0.5}Zn_{0.5}Fe_2O_4$ at optimized reaction conditions measured up to 100 h. The inset displays the weight hour space velocity (WHSV) dependence at TOS = 8 h for conversion and product selectivity. Fig. 6 demonstrates that aniline conversion decreased with increasing WHSV; however, DMA formation became considerable at lower WHSV (or higher contact time), indicating a longer residence time of NMA on the catalyst surface, leading to consecutive methylation and hence declining NMA selectivity. Similarly, a small amount of orthotoluidine formed only at the lowest WHSV value used, suggesting that it was likely due to the isomerization of NMA. At higher WHSV, NMA formed exclusively and selectively, although aniline conversion was poor. An optimum of 58% aniline conversion with nearly 98% NMA selectivity was achieved at WHSV = 3.58 h^{-1} (or contact time = 0.28 h). This above optimized WHSV was fixed for all studies.

3.4. *XPS analysis*

Fresh and spent catalysts (after methylation at 573 K for 4 h with a 3:1:1 feed composition of CH_3OH:$PhNH_2$:H_2O and WHSV = 3.58 h^{-1}) were analyzed by XPS. A careful comparison of aniline conversion data on all catalyst compositions

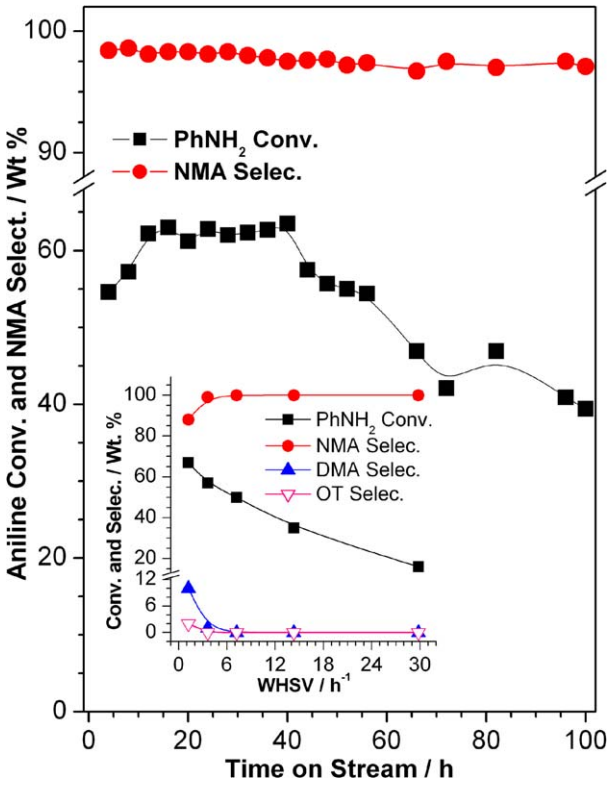

Fig. 6. Time-on-stream and weight hour space velocity (inset) dependence of aniline conversion and NMA selectivity on $Cu_{0.5}Zn_{0.5}Fe_2O_4$ at 573 K, with 3:1:1, CH_3OH:$PhNH_2$:H_2O, WHSV = 3.58 h^{-1}.

(Fig. 4) indicates the onset of decreased activity at TOS = 4–5 h, except on $x = 0.5$. XRD of spent catalysts ($x = 0.05$ and 0.25) showed Cu^0 formation after TOS = 8 h. Further analysis of the spent catalysts at TOS > 8 h showed a high coke content, except on $x = 0.5$, and provided no significant new information. Hence an analysis of the spent, but still active, catalysts after 4 h of reaction and a comparison of all catalysts could give a better indication of changes occurring due to the reaction.

3.4.1. *Cu 2p core-level and Cu $L_3M_{45}M_{45}$ spectra*

Cu 2p core-level photoemission spectra from calcined and spent $Cu_{1-x}Zn_xFe_2O_4$ catalysts are shown in Fig. 7. XPS and XAES results from Cu $2p_{3/2}$ core level and Cu-LMM Auger transitions, respectively, are summarized in Table 2. All calcined samples exhibited Cu $2p_{3/2}$ main line at 934.2 ± 0.2 eV with FWHM = 3 eV, indicating that the electron density on Cu remained the same irrespective of the amount of Zn present. Good satellite intensity (I_s) was observed around 942 eV for all x values, indicating the existence of Cu^{2+} ions. The intensity ratio between satellite and main line (I_s/I_m) was 0.45–0.55 in all cases, very close to that of pure CuO [31–34].

The XPS results of Cu $2p_{3/2}$ core level from spent catalysts are interesting and reveal some new features compared with fresh catalysts. Considerable broadening (FWHM = 4 eV) was observed with satellites for $x = 0.5$ and 0.75; however, a relatively sharp feature at lower BE with a shoulder on the higher BE and weak I_s were observed for $x = 0.05$ and 0.25. A de-

Table 2
XPS and XAES parameters from $Cu_{1-x}Zn_xFe_2O_4$

x	BE of Cu $2p_{3/2}$ (FWHM) eV		KE of Cu LMM		α' (eV)	
	Fresh	Spent	Fresh	Spent	Fresh	Spent
0.05	934.1 (3.0)	932.1, 933.8 (4.0)	917.7	918.6, 917.0	1851.8	1850.7, 1850.8
0.25	934.4 (3.0)	932.2, 933.5 (4.1)	917.5	918.5, 917.0	1851.9	1850.7, 1850.5
0.50	934.2 (3.0)	932.1 934.1 (3.8)	917.5	917.2	1851.7	1849.3, 1851.3
0.75	934.4 (3.0)	932.2, 933.9 (3.5)	917.1	916.5, 917.3	1851.5	1848.7, 1851.2

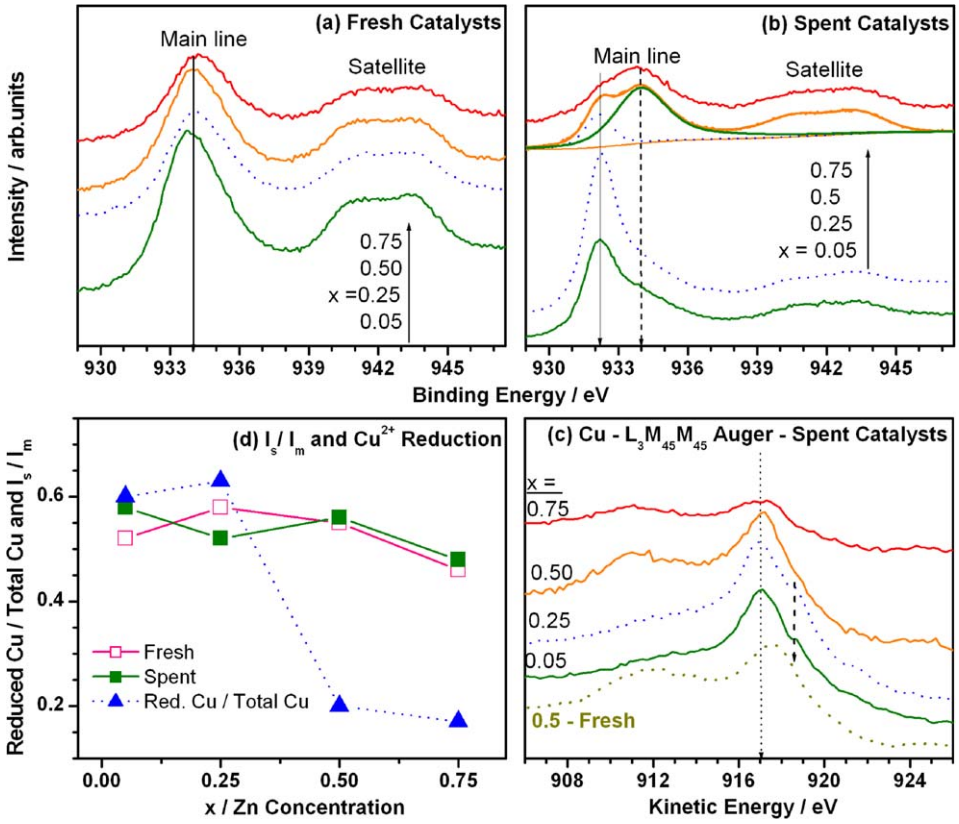

Fig. 7. Cu $2p_{3/2}$ core level photoemission spectra from (a) fresh and (b) spent $Cu_{1-x}Zn_xFe_2O_4$ catalysts. Cu $2p_{3/2}$ core level from $x = 0.5$ (spent) spectrum was deconvoluted to show the presence of reduced Cu-species. (c) Cu-LMM spectra from spent $Cu_{1-x}Zn_xFe_2O_4$ catalysts. (d) I_s/I_m for the fresh and spent catalysts and the ratio of reduced Cu-species to that of total Cu on spent catalyst. Note the marked decrease in the reducibility of $x = 0.5$ and 0.75 compositions.

convolution for $x = 0.5$ (Fig. 7b and Table 2) reveals the contribution from a new peak at lower BE (932.2 eV) by reduced Cu species. For $x = 0.05$ and 0.25, the I_s at higher BE appeared weak. An important point to note is the partial reduction of Cu^{2+} ions during the course of the reaction. Nonetheless, the extent of reduction decreased with increasing Zn concentration.

Reduced Cu species (Cu^0 and Cu^+) cannot be distinguished by XPS, because they appeared at the same BE with no satellite features. Nevertheless, the valence states of reduced Cu species can be easily distinguished using XAES, because the Cu^+ and Cu^0-$L_3M_{45}M_{45}$ (LMM) appeared at around 916.5 and 918.5 eV, respectively [35]. The Cu-LMM Auger spectra of spent catalysts and $x = 0.5$ calcined catalyst are given in Fig. 7c, and the results are summarized in Table 2. Note that the fresh catalyst with $x = 0.5$ exhibited an LMM line at a KE of 917.7 eV, which is very close to that of CuO at 917.6 eV [35]. However, on other calcined catalysts, this value decreased up to 917.1 eV. On spent catalyst of $x = 0.05$ and 0.25, the Cu-LMM transition can be observed with a relatively sharp peak at 917.0 eV, which is intermediate between Cu_2O and CuO and a shoulder at 918.5 eV, typical of Cu^0. These findings are in line with the XRD results, which showed metallic Cu. Note that the Cu^0 on the surface can be readily oxidized to Cu_2O in the atmosphere, which could explain the above intermediate KE at 917 eV. However, at $x = 0.5$ and 0.75, a broad peak structure is exhibited at high KE (917.2 eV). The fresh catalysts also exhibited a single peak around 917.4 ± 0.2 eV in this region. This clearly indicates an increasing contribution of Cu^{2+} at higher x; however, the broadening indicates the contribution of Cu^+ species at low KE. The Auger parameter (α') [35] calculated for spent catalysts was 1851.2 eV for $x = 0.5$ and 0.75, indicating a major contribution of Cu^{2+}. Overall, the significant reduction in the form of Cu (and some Cu^+) on $x = 0.05$ and 0.25, along with limited reduction to

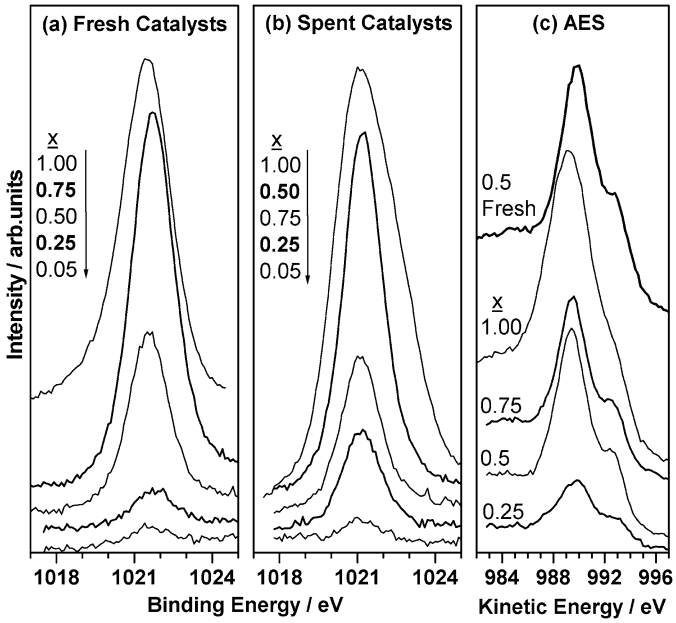

Fig. 8. Zn $2p_{3/2}$ core level photoemission spectra from (a) fresh and (b) spent $Cu_{1-x}Zn_xFe_2O_4$ catalysts. (c) Zn-LMM spectra from spent $Cu_{1-x}Zn_xFe_2O_4$ catalysts. Note the difference in stacking on panel b and a high intensity feature for $x = 0.5$ and a broadening for $x = 1$.

Table 3
Binding Energy and FWHM of Zn $2p_{3/2}$ core level on fresh and spent $Cu_{1-x}Zn_xFe_2O_4$ catalysts

x	BE of Zn $2p_{3/2}$ (FWHM) eV	
	Fresh	Spent
1	1021.4 (2.3)	1021.1 (2.9)
0.75	1021.7 (1.9)	1021.1 (1.8)
0.5	1021.5 (1.8)	1021.2 (1.8)
0.25	1021.7 (1.8)	1021.2 (1.8)
0.05	1021.5 (2.3)	1021.1 (2.7)

Cu^+ along with most of the Cu^{2+} on $x = 0.5$ and 0.75, are clearly shown.

The I_s/I_m of fresh and spent catalysts and the reducibility of Cu calculated as the percentage of reduced Cu species to total Cu content is given in Fig. 7d. This reducibility shows a sudden decrease from $x = 0.05/0.25$ to $x = 0.5/0.75$. It is apparent that the large amount of Zn prevented the reduction of Cu^{2+}. The I_s/I_m of fresh and spent catalyst systems are very close, indicating that the nature of unreduced Cu^{2+} remains the same.

3.4.2. Zn 2p core-level and Zn-$L_3M_{45}M_{45}$ spectra

The Zn 2p core-level spectra and Zn-$L_3M_{45}M_{45}$ Auger spectra are given in Fig. 8 for fresh and spent catalysts. Zn-LMM results from spent catalyst are given, along with calcined $x = 0.5$ catalyst for comparison. The BE and FWHM of Zn $2p_{3/2}$ core-level spectra are summarized in Table 3. All of the fresh catalysts exhibited a peak centered at 1021.6 ± 0.1 eV, which is very close to the BE of ZnO (1022 eV) [35]. Zn $2p_{3/2}$ peak appeared at 1021.2 eV for all spent catalyst compositions, demonstrating a significant shift in BE compared with the fresh catalysts. This also hints at the possibility of significant but similar changes occurring under reaction conditions. The noticeable increase in FWHM observed may indicate a possible contribution from two types of Zn species on $ZnFe_2O_4$. However, Zn-LMM XAES of all spent catalysts showed a main line KE feature at around 989.5 eV due to Zn^{2+}, because the metallic Zn Auger line appeared at ~992 eV [34]. The α' calculated for Zn^{2+} (2010.1–2011 eV) on the spent catalysts also confirms the existence of Zn^{2+} and not that of metallic Zn (2014 eV). However, α' was different for the fresh $x = 0.5$ catalyst, observed at 2011.5 eV. A shift in the BE of Zn 2p might be due to a change in the environment around Zn on spent catalysts resulting from the partial reduction of other metal ions.

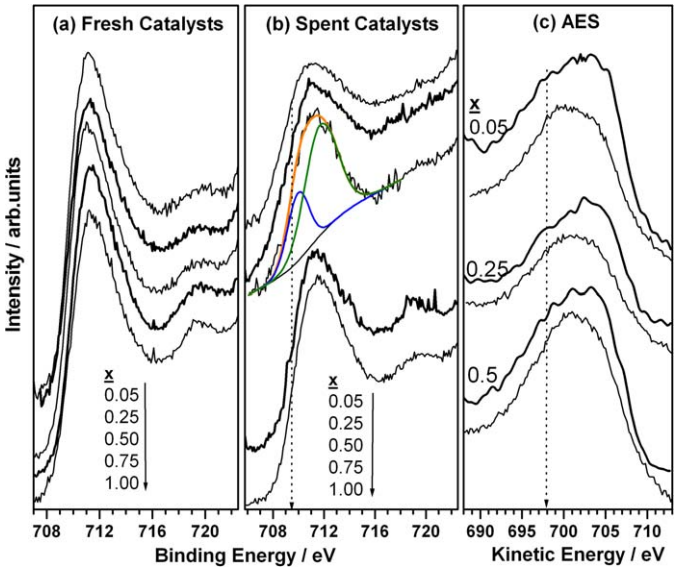

Fig. 9. Fe 2p core level XPS of (a) fresh and (b) spent $Cu_{1-x}Zn_xFe_2O_4$ catalysts. A shoulder is seen below 710 eV on spent catalysts (dotted line) indicates a partial reduction of iron. Deconvolution of Fe $2p_{3/2}$ peak for $x = 0.5$ demonstrates Fe^{2+} and Fe^{3+} on spent catalysts. (c) Fe-LMM Auger spectra of selected fresh and spent catalysts.

3.4.3. Fe 2p core-level and Fe-$L_3M_{45}M_{45}$ spectra

Photoemission core-level spectra of Fe $2p_{3/2}$ are given in Figs. 9a and b for fresh and spent catalysts, respectively. The following important points are noted:

(i) A clear satellite around 719 eV with a $2p_{3/2}$ main line centered at 711.2 eV was observed due to the predominant Fe^{3+} on fresh catalysts; however, a weak I_s was observed on the spent catalysts with $x \leqslant 0.5$.
(ii) The spent catalysts displayed a shoulder at 709.7 eV, characteristic of Fe^{2+} species, for catalysts with $x \leqslant 0.5$ [36,37]. A peak deconvolution for $x = 0.5$ clearly shows the contribution from Fe^{2+}. The intensity of Fe^{2+} decreased with increasing bulk Zn content, and no reduction was observed on $ZnFe_2O_4$.

Fe-$L_3M_{45}M_{45}$ spectra for catalysts with $x \leqslant 0.5$ are given in Fig. 9c. The spent catalyst spectra were normalized to fresh catalyst spectra for better presentation. The fresh catalyst spectra

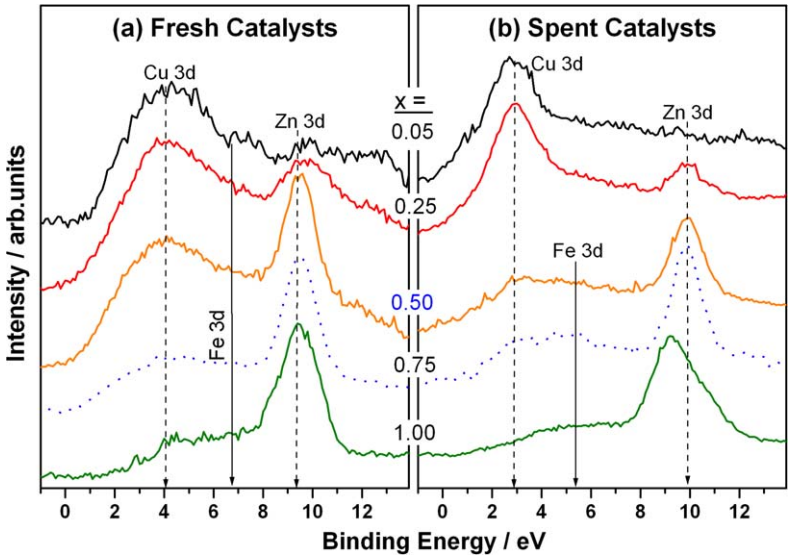

Fig. 10. Valence band XPS of (a) fresh and (b) spent $Cu_{1-x}Zn_xFe_2O_4$ catalysts. Note a decrease (increase) in the BE of Cu 3d (Zn 3d) level on spent catalysts compared to fresh, except $x = 1$.

are similar, with peaks centered at KE 701.5 eV and no significant differences observed. A considerable change was clearly seen on the spent catalysts, especially those with $x = 0.05$ and 0.25. A shoulder seen at KE 698 eV (dotted arrow) was ascribed to Fe^{2+}; however, the intensity of this feature was lower at $x = 0.5$. These results for Fe-$L_3M_{45}M_{45}$ indicate a partial reduction of Fe^{3+}, with the extent of reduction decreasing with increasing x, as observed for Fe 2p core-level spectra.

3.4.4. Valence band photoemission

XPS spectra of the valence band (VB) region obtained from the fresh and spent $Cu_{1-x}Zn_xFe_2O_4$ catalysts are shown in Fig. 10. The main VB appearing at <8 eV include contributions from 3d bands of Cu and Fe and 2p bands of O. At the $h\nu = 1253.6$ eV used in these experiments, the photoionization cross-section (σ) value (Cu 3d = 0.021; Fe 3d = 0.0045; O 2p = 0.0005 Mb) [38] is the dominating factor in determining the spectral intensity. The above data suggest that Cu 3d should make a large contribution to the VB and that the contribution from O 2p is negligible. The VB assignments are straightforward from the intensity and the BE of the bands. High-intensity VB observed around 4 eV corresponds to Cu 3d, and its intensity decreased with increasing value of x in the fresh catalysts. A low-intensity broad band was observed at 4–7.5 eV, due to the contribution from Fe 3d and O 2p bands. A completely filled Zn 3d band was observed far away from the main VB, at 9.4 eV; its intensity increased linearly with increasing value of x.

Significant changes observed from core levels of spent catalysts are reflected strongly in the VB spectra as well. The main observations are as follows:

(i) The Cu 3d band shifted to lower BE by 1 eV (dotted arrow at 3 eV) accompanied by a narrowing of the band on $x = 0.05$ and 0.25, whereas for the $x = 0.5$ and 0.75 systems, the Cu 3d band was very broad and centered at 4 eV.
(ii) A shift in the Fe 3d level of about 1 eV was clearly seen.
(iii) The Zn 3d band shifted marginally to higher BE (dotted arrow at 10 eV) for $0.25 \leqslant x \geqslant 0.75$ systems, but remained centered at 9.2 eV with an asymmetric broadening for $ZnFe_2O_4$.

The above points suggest that the changes in Cu and Fe VB were significant on the spent catalysts. However, comparing the BEs of the Zn 3d band on the fresh (9.4 eV) and spent catalysts (10 eV) suggests that Zn might be in a significantly different environment, due to the partially reduced metal ions on spent catalysts.

3.4.5. Catalyst surface composition

The metal ion ratios on the surface of all of the catalyst systems are given in Table 4. This information aids understanding of the metal ion distribution and the heterogeneity of these ions on the surfaces that directly influence catalytic activity. A linear relationship existed between the surface metal ion content and the nominal metal ion input amount (x) on all fresh catalysts (Table 4). In contrast, a dramatic change in surface compositions was observed on spent catalysts. A high Cu/Fe (>1) was found on spent catalysts, after 24 h on TOS, with $x = 0.05$ and 0.25, whereas the $x = 0.5$ and 0.75 systems exhibited Cu/Fe < 1. The $x = 0.5$ spent catalyst was also subjected to XPS study, due to its stable catalytic activity; the Cu/Fe ratio decreased from 0.72 (TOS = 4 h) to 0.57 (TOS = 24 h). An appreciable increase in Zn/Fe ratio was observed from fresh (0.20) to spent (0.58) catalyst with $x = 0.5$ (TOS = 4 h); this subsequently decreased to 0.40 after TOS = 24 h. Both the Cu/Fe and Zn/Fe ratios decreased for the $x = 0.5$ system at 24 h after the initial hours (4 h) of the reaction, indicating a continuous change in metal ion concentration on the surface during the transient reaction period of the first 12 h, followed by stabilization (Figs. 4 and 6). Further, a (Cu + Zn)/Fe ratio of <1 for all of the fresh samples indicates a somewhat Fe-dominated surface character before the reaction. Nonetheless, an increase

Table 4
Surface atomic ratio calculated from photoemission studies on fresh and spent $Cu_{1-x}Zn_xFe_2O_4$ catalysts

x	Fresh				Spent[a]				Spent		
	Cu/Zn	Cu/Fe	Zn/Fe	(Cu + Zn)/Fe	Cu/Zn	Cu/Fe	Zn/Fe	(Cu + Zn)/Fe	Cu/C	Zn/C	Fe/C
0.05	68.55	0.86	0.01	0.87	34.2	1.25	0.04	1.29	0.35	0.01	0.28
0.25	13.43	0.74	0.05	0.79	7.42	1.47	0.20	1.67	0.50	0.07	0.34
0.5	2.81	0.54	0.20	0.73	1.25	0.72	0.58	1.30	0.48	0.38	0.66
0.5[b]	–	–	–	–	1.48	0.57	0.40	0.97	0.55	0.37	0.96
0.75	0.79	0.37	0.47	0.84	1.38	0.62	0.45	1.10	0.17	0.12	0.27
1	–	–	1.00	1.00	–	–	1.20	1.20	–	0.77	0.64

[a] Spent catalyst collected at TOS = 4 h.
[b] Spent catalyst collected at TOS = 24 h.

in (Cu + Zn)/Fe of >1 for all spent catalysts hints at enriched Cu and/or Zn on the surface due to reaction and a substantially diminished role of Fe.

The contribution of Cu to the (Cu + Zn)/Fe ratio was significant, as evident from the Cu/Fe ratio for $x \leqslant 0.75$. At TOS = 24 h, the (Cu + Zn)/Fe ratio on the surface of $x = 0.5$ was close to unity (0.97), indicating optimum heterogeneous distribution of all metal ions on the surface. A significant amount of carbon deposition is also evident from the ratios of metal ions and C; however, carbon deposition was relatively lower on $x = 0.5$ and 1. Interestingly, the catalyst with $x = 0.5$ at TOS = 24 h showed the highest metal/C ratio of all compositions. High C and low Zn concentrations were observed, as evident from Zn/C, on $x = 0.05$, 0.25, and 0.75, irrespective of bulk concentration.

Fig. 11 displays the (Cu + Zn)/Fe, (Zn/Fe for $x = 1$) ratio calculated from XPS results (a) and aniline conversion with NMA yield for all of the compositions (b). Interestingly, with a (Cu + Zn)/Fe ratio close to 1 (dotted line in Fig. 11a), in general the aniline conversion is reasonably good. This might be why all of the Cu-containing catalysts exhibited high conversion in the first few hours of the reaction. However, the ratio changes with time, and at the onset of deactivation (TOS = 4 h), it reflects the state of the surface composition. Clearly, a redistribution of metal ions on the surface occurred as the reaction progressed on all of the compositions. Although the same (Cu + Zn)/Fe ratio was observed for $x = 0.05$ and 0.5 (TOS = 4 h), the nature of Cu species changed from dominantly Cu^{2+} on $x = 0.5$ to reduced Cu species on $x = 0.05$. Further, the increased (Cu + Zn)/Fe ratio was almost entirely due to an increase in the Cu content on $x = 0.05$, leading to Cu agglomeration and sintering, as observed in the XRD results (Fig. 1b). Although the $x = 0.75$ spent catalyst exhibited an atomic ratio of 1.1, the amount of carbon deposition was high (Table 4), and hence the active metal content on the surface was low. Nonetheless, the somewhat stable activity for $x = 0.75$ correlates well with a (Cu + Zn)/Fe ratio close to 1. These observations hint at the need for a sufficient concentration of oxidized Cu^{2+} for sustainable alkylation activity. Only on $x = 0.5$ (TOS = 24 h) was the (Cu + Zn)/Fe ratio maintained at 1 and hence extended catalytic activity observed. Clearly, it is not a single metal ion, but rather the heterogeneity of the surface (specifically, a combination of all three metal ions), that brings out the desired reactivity

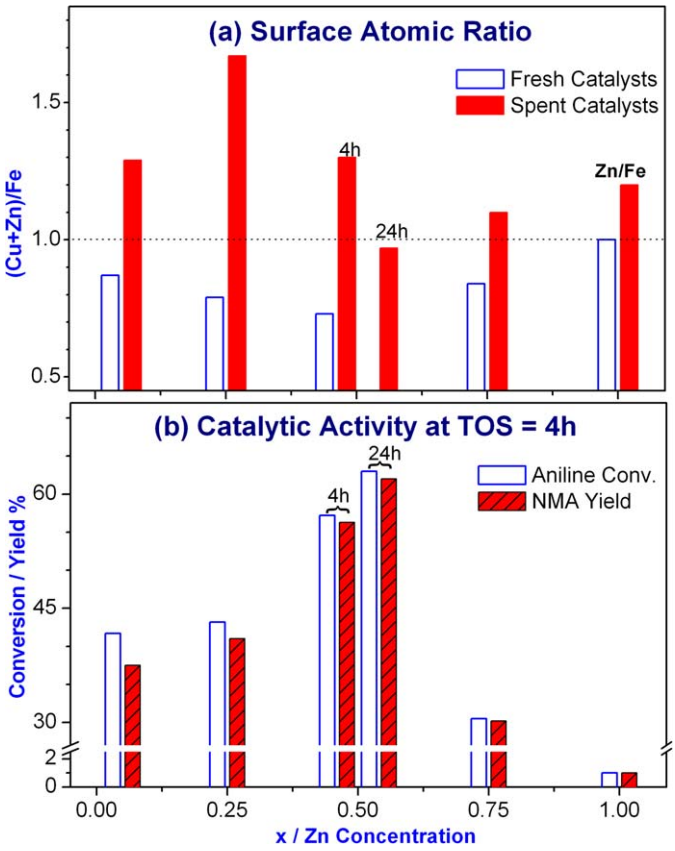

Fig. 11. Comparison of (a) atomic ratio of (Cu + Zn)/Fe for all fresh and spent catalyst compositions and (b) aniline conversion and NMA selectivity on $Cu_{1-x}Zn_xFe_2O_4$ catalysts. Note the (Cu + Zn)/Fe ≈ 1 after 24 h of reaction on $x = 0.5$ and stable catalytic activity associated with it.

with stability. Our earlier reports on FTIR studies [25,26] also support the above arguments.

4. Discussion

4.1. Catalytic performance

Systematic investigations on $A_{0.5}A'_{0.5}Fe_2O_4$ led to the highly active and selective $Cu_{1-x}Zn_xFe_2O_4$ system toward the production of NMA by aniline methylation. Aniline N-methylation with methanol led selectively (>96%) to NMA on $Cu_{0.5}Zn_{0.5}Fe_2O_4$ catalyst with stable activity under optimized reaction conditions. Facile NMA formation from per-

pendicularly oriented aniline on the above composition [25,26] indicates that this is a promising system for this reaction, although the maximum aniline conversion is 60–65% and worth pursuing. However, aniline conversion and/or NMA selectivity decreased when moving either side of the above optimum conditions, in terms of high/low reaction temperatures, WHSV, and catalyst composition. It is evident that DMA forms at the expense of NMA at high reaction temperatures and high contact times. This indicates a sequential methylation mechanism, with dimethylation rate increasing considerably with temperature. In addition, catalysts deactivate faster with TOS at higher temperatures, due mainly to SRM, which reduces the active Cu^{2+} to Cu^0 (Figs. 2b and 7).

The very low aniline conversion observed on $x = 1$ is due mainly to poor interaction among the reactants on the catalyst surface, as was clearly shown in our earlier IR reports [25,26]. In contrast, samples with $x = 0.05$ and 0.25 deactivate faster, due to a higher degree of SRM to H_2, which reduces Cu^{2+} active species to Cu^0, whereas on increasing Zn ($x \geqslant 0.5$) concentration, Cu^{2+} reduction is mainly avoided, as is evident from the Cu 2p core-level XPS (Figs. 2, 4, and 7). Introducing Zn into the $CuFe_2O_4$ systems enhances the catalyst lifetime. In contrast, introducing Cu into the $ZnFe_2O_4$ systems causes an increase in aniline conversion by up to two orders of magnitude. This demonstrates that the active site for methylation is indeed Cu^{2+}. However, adding Zn improves catalyst stability, even though Zn does not exhibit significant activity.

Aniline conversion and NMA selectivity vary quite considerably, depending on the methanol:aniline ratio in the feed (Fig. 3). Mixed metal oxides of $CuO–Fe_2O_3$, $ZnO–Fe_2O_3$ [39], and $CuO–ZnO–Al_2O_3$ [40] catalysts are well known for methanol gasification reactions and support our findings that an excess amount of methanol in the feed is necessary. An optimum methanol:aniline ratio of 3 is needed to operate at high NMA selectivity with intermediate aniline conversion with the lowest extent of methanol gasification reaction possible.

Temperature influences the methylation kinetics to a large extent; an appreciable increase in aniline conversion was observed on increasing the temperature from 543 to 573 K, with a negligible decrease in NMA selectivity (Fig. 5). A further increase in temperature affected NMA selectivity due to the formation of DMA and OT, with a notable drop in aniline conversion. There are few reasons for this change in catalytic activity at high temperature. IR studies have clearly shown that aniline desorbs at around 573 K [25,26], which is partly responsible for the low aniline conversion above 573 K. Almost the same catalytic activity was resumed at 573 K after carrying out the reaction at 633 K, indicating that high aniline desorption at high temperature plays a significant role in aniline conversion. Significant inevitable methanol gasification/SRM at high temperature led to poor methanol availability and hence low NMA yield. The general observation of reduced metal ions on the spent catalyst shows that the overall reaction occurs under moderate to marginal reduction conditions, depending on the Cu content. It is obvious that SRM or MeOH gasification is highly plausible at high temperatures, and the role of the present Lewis acid catalyst is to suppress the above reaction. Clearly, Zn suppresses these reactions on $Cu_{1-x}Zn_xFe_2O_4$, and the same is clearly indicated from the general decrease in carbon content with increasing Zn content.

4.2. Electronic structure and distribution of metal ions on $Cu_{1-x}Zn_xFe_2O_4$

The spent catalysts showed a predominant spinel phase with small amounts of Cu^0 on Cu-rich compositions, due to the reductive atmosphere under methylation conditions. Nonetheless, the Cu^+ observed in XPS on all compositions indicates the possibility that either the surface Cu^0 clusters were oxidized due to aerial oxidation or that Cu^{2+} ions were partially reduced due to reaction. However, coke deposition prevents oxidation of metal species in the bulk, and diffraction corresponds to Cu metal, as shown on XRD. This also indicates the inevitable structural change to some extent at $x = 0.05$; nevertheless, Cu^{2+} reduction was observed at a less significant level for catalysts with $x > 0.25$, as evident from the absence of metallic reflections on XRD. Surface area decreased after the reaction for all of the compositions except $x = 0.5$, likely due to surface agglomeration of metal ions and/or deposition of coke on the surface, as evident from the surface atomic composition results (Table 4). The $x = 0.05$, 0.25, and 0.75 systems exhibited significantly decreased surface area, as well as high deposited carbon content. Note that the increased crystallite size in the spent catalysts led to the decreased surface area. Nevertheless, only the $x = 0.5$ composition retained its textural properties, and the reaction had no significant influence on its structural integrity. This also hints that the spinel can accommodate some reduced metal ions without undergoing structural collapse.

Several discrepancies observed between the fresh and spent catalysts reveal the changes in the oxidation state of the metal ions occurring under experimental conditions. The main XPS findings were decreased Cu^{2+} reducibility with increasing Zn content and an unambiguous redistribution of metal ions on the surface of spent catalysts, depending on the catalyst composition. As evident from the surface atomic ratio for the better-performing $x = 0.5$ spent catalyst, the Cu/Fe ratio increased marginally with increasing Zn/Fe ratio, indicating an optimum distribution of active Cu^{2+} surrounded by Zn and Fe. However, for Cu-rich compositions, the Cu/Fe ratio increased significantly, indicating a high probability for agglomeration of Cu as the reaction proceeds, leading to faster deactivation for these compositions. In contrast, on the $x = 0.5$ system, the Zn content also increased, hindering Cu aggregation; a (Cu + Zn)/Fe ratio close to unity perfectly supports sufficient separation of all of the metal ions, so that no metal ion meets a similar ion in the near-neighbor environment. This could be one reason for the high and stable catalytic activity observed with $x = 0.5$. An increase in Fe content also occurred (TOS = 24 h for $x = 0.5$) on the surface to maintain the initial structural integrity of the catalytic system. This might be due to a reaction-induced change in surface composition in the first 12 h, followed by stable activity for up to 60 h (Fig. 6). As shown by Cu 2p photoemission on the $x = 0.5$ system at different TOS (Fig. 12), the active Cu^{2+} and structural integrity of the system were retained

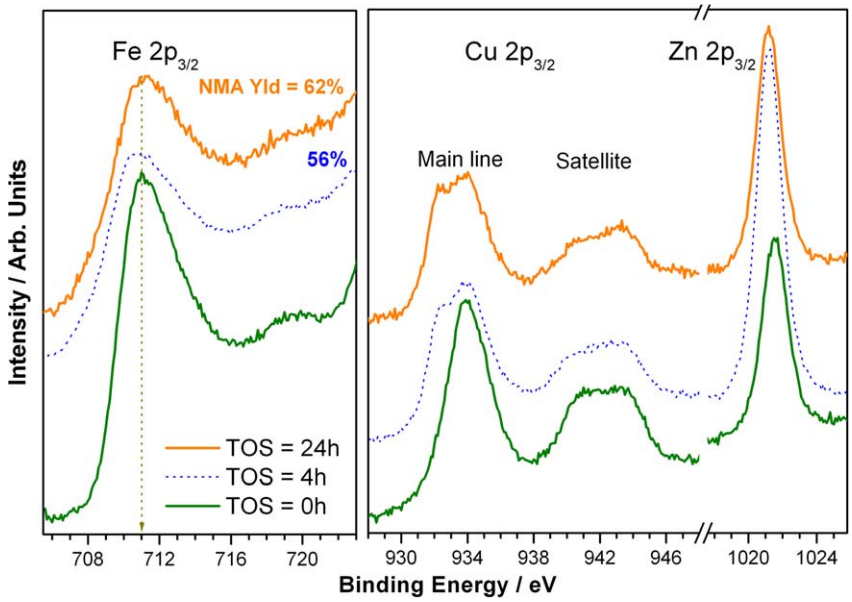

Fig. 12. A comparison of Fe 2p, Cu 2p and Zn 2p core level features on fresh and after two different stages of reaction on $Cu_{0.5}Zn_{0.5}Fe_2O_4$ catalyst. Note a drastic change in the transition metal content accompanied with some reduction after different stages of reaction.

even after 24 h. Except for some Cu^+ formation after the initial reaction period, the overall Cu content remained the same on the surface throughout the reaction. It is the change in Zn and Fe content on the surface that kept the average surface atomic composition constant and helped to maintain the activity for a longer period. These findings lend reiterate the concept that the heterogeneity of all metal ions determines the stability of the catalyst. Although (Cu + Zn)/Fe was close to unity on $x = 0.75$, the decreased aniline conversion was due mainly to the very high C content, as reflected in the ratio of metal ions to C (Table 4).

Although XPS and XAES results were explained earlier, a Wagner plot [41] shown in Fig. 13 makes identification of the different reduced species easier. KE of Auger transition on the y-axis and the Cu $2p_{3/2}$ BE on the x-axis are plotted in Fig. 13 for all of the catalysts. The data for Cu, Cu_2O, and CuO [42] are also plotted in this figure. The Auger parameters are described by a solid straight line with a slope of −1. The figure clearly shows that Cu^{2+} in all of the fresh and spent catalysts were similar to that of CuO. Indeed, the $x = 0.5$ and 0.75 systems more closely resembled CuO than the $x = 0.05$ and 0.25 systems. The nature of reduced species on the $x = 0.05$ and 0.25 systems corresponded to that of Cu^0; however, the same corresponded to Cu_2O-like species on the $x = 0.5$ and 0.75 systems.

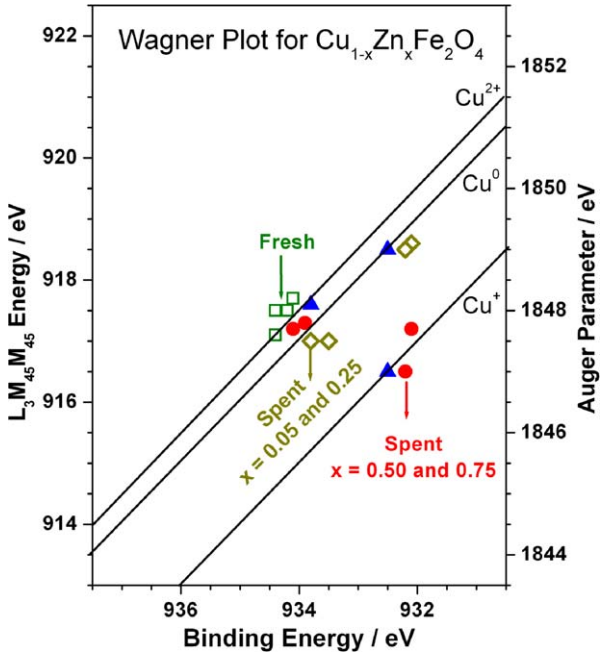

Fig. 13. Wagner plot for $Cu_{1-x}Zn_xFe_2O_4$ catalysts from the Cu $2p_{3/2}$ core level and Auger spectral data. Data points for standard compounds (Cu, Cu_2O and CuO) are given by solid blue triangles and fresh catalyst by open green squares. Spent catalysts with $x = 0.05$ and 0.25 composition indicated by open dark yellow squares and $x = 0.5$ and 0.75 by solid red color circles, respectively. The Auger parameter is described by solid straight line with a slope of −1. Nature of reduced Cu-species is dominantly Cu^0 on $x = 0.05$ and 0.25 and Cu^+ on $x = 0.5$ and 0.75.

4.3. Zn^{2+}, an "active spacer" on catalyst and stabilizer toward reaction

XPS and XRD results in the present study reveal that Cu-rich systems, $x = 0.05$ and 0.25, exhibited a significant Cu^{2+} reduction and agglomeration due to SRM and H_2 production. In contrast, for $x = 1$, no such dramatic changes were observed with Zn. However, at intermediate composition ($x = 0.5$), Cu^{2+} reduction to metal was totally suppressed and the catalytic activity was maintained for a longer period. The large energy gap observed between the Cu or Fe 3d and Zn 3d bands (Fig. 10) suggests that it had hardly any electronic interaction. Note that there was no reduction of Fe^{3+} to Fe or Fe_xC_y, as in the case of the closely related $Cu_{1-x}Co_xFe_2O_4$ used for phenol ethylation [27]. Further, the surface atomic composition results clearly indicate that both Cu and Zn content on the surface

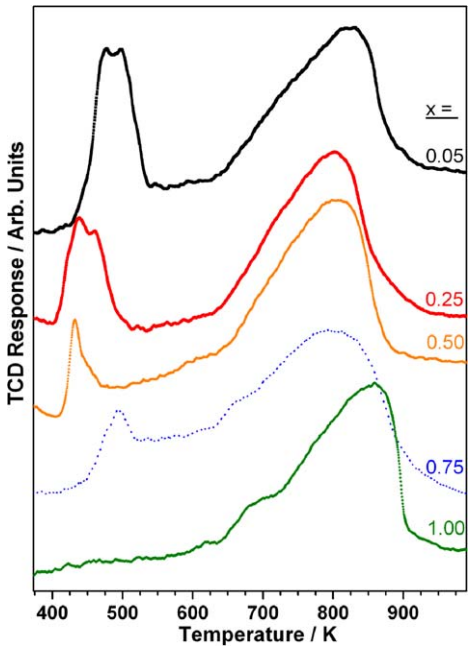

Fig. 14. TPR profiles of $Cu_{1-x}Zn_xFe_2O_4$ catalysts measured with 5% H_2 in Argon, under a flow rate of 30 ml/min at a heating rate of 5 K/min. A continuous H_2 consumption between 525 and 650 K to be noted on $x = 0.5$ and 0.25.

changed significantly for the $x = 0.5$ system as the reaction proceeded in the first 12 h, after which an almost a 1:1 combination of Cu and Zn was maintained on the catalyst surface. The change in surface atomic composition, a transient change in catalytic activity up to 12 h before it reached stable activity, and a comparison of deactivation trend and surface atomic composition of other catalyst compositions clearly indicate the role of Zn as an "active spacer" on $Cu_{0.5}Zn_{0.5}Fe_2O_4$ that helps prevent the reduction/agglomeration of Cu^{2+} under the present experimental conditions. A considerable increase in the lattice constant for $x = 0.5$ (Table 1) supports the view that the lattice can accommodate Cu^+ ions to certain degree without undergoing structural collapse. Because the role of Zn-spacer increases marginally and helps maintain the catalytic activity in the present system, we call it an "active spacer," in contrast to the lower activity observed when any spacer is introduced in a catalytic system. The low aniline conversion at $x = 1$ changed dramatically with the addition of Cu at $x = 0.5$, demonstrating the prime importance of Cu in aniline methylation and the combined effect of Cu + Zn in overall catalyst performance. The synergetic performance of Cu and Zn plays major roles in aniline methylation and catalyst stability.

A final support to the active spacer role in preventing the reduction of Cu^{2+} is obtained from TPR experiments, as shown in Fig. 14. All of the Cu-containing $Cu_{1-x}Zn_xFe_2O_4$ compositions clearly show a Cu reduction peak at around 473 K and Fe and Zn reduction features in a broad peak between 650 and 900 K. The Cu^{2+} reduction peak at around 475–500 K for $x = 0.05$ and 0.75 shifts to lower temperatures (425–450 K) for $x = 0.25$ and 0.5. Note that various Cu^{2+} reduction peaks have been observed in mixed Cu–Zn–Al oxide system, and that the Cu^{2+} reduction temperature is highly dependent on Zn content in this system [43–45]. Careful analysis also revealed that the amount of H_2 uptake decreased nonlinearly with decreasing Cu content. A quantitative analysis of the results for the $x = 0.5$ (0.05) systems hints that the amount of H_2 uptake in the temperature range of 413–500 K (425–525 K) corresponds to a Cu^{2+} to Cu^+ (Cu^{2+} to Cu^0) reduction. A further careful look at the $x = 0.5$ trace reveals a continuous H_2 uptake, at a lower level, between 523 and 653 K. A similar H_2 uptake pattern can be seen for $x = 0.25$, at a still-lower intensity level; however, this feature was not observed on the (Cu-rich) $x = 0.05$ composition, indicating the complete reduction to Cu^0 at 525 K. This clearly supports the conclusion that total Cu^{2+} reduction occurred only above 573 K on the $x = 0.5$ composition due to the active spacer role of Zn. However, a partial reduction to Cu^+ clearly occurred, as was also observed on XPS. More detailed analysis on TPR will be published elsewhere.

5. Conclusion

A systematic investigation of the selective production of NMA from aniline led to the identification of Cu^{2+}-containing ferrite catalysts as potential candidates. Further studies on Cu–Zn mixed ferrite exhibited stable activity for longer periods. This paper has reported the results from the catalytic study of selective NMA production from aniline methylation on $Cu_{1-x}Zn_xFe_2O_4$ over a wide range of temperatures and catalyst compositions with a methanol:aniline molar ratio of 3. Although all of the catalyst compositions produced NMA selectively at 573 K, only the $x = 0.5$ composition exhibited maximum aniline conversion under optimum reaction conditions. All of the Cu-containing compositions showed high initial activity; however, activity decreased with increasing TOS for all but the $x = 0.5$ composition. $ZnFe_2O_4$ showed hardly any catalytic activity, hinting that Zn and Fe have negligible direct roles. Cu seems to be the active species for aniline methylation. Detailed catalytic activity studies showed that Cu^{2+} was largely responsible for methylation and that Zn^{2+} enhanced the stability of the system, whereas $ZnFe_2O_4$ displayed no significant activity toward methylation on its own.

Photoemission studies were carried out to address the change in activity with catalyst composition and to identify a structure–activity correlation. The fresh catalysts clearly exhibited Cu^{2+}, Zn^{2+}, and Fe^{3+} species; however, the spent catalysts showed composition-dependent oxidation states. A significant reduction of Cu^{2+} to Cu was observed for the $x \leqslant 0.25$ system. The above total reduction was fully suppressed on $x = 0.5$ and 0.75; however, partial reductions of Cu^{2+} to Cu^+ and of Fe^{3+} to Fe^{2+} were observed. The valence band showed a significant change in BE of the 3d bands of Cu and Fe on the spent catalysts. Redistribution of cations on the spinel surface during reaction conditions was also evident from the surface composition analysis. The redistribution of metal ions on the surface determines the course of the reaction. The presence of almost equal amounts of Cu and Zn on the surface is needed for longer TOS methylation activity on these spinel systems, in which Cu^{2+} is the active species for methylation and Zn^{2+} acts as an active spacer to decrease the extent of Cu^{2+} reduction and Cu

agglomeration on the surface. Complete heterogeneity of the surface metal ion composition aids stable catalytic activity and retention of the structural integrity of the catalyst.

Acknowledgments

The authors thank Prof. A.V. Ramaswamy for helpful discussions on TPR results and for a critical reading of the manuscript, Dr. Veda Ramaswamy for providing the GC facility, and Dr. S.P. Mirajkar for the TPR experiments. M.V. thanks CSIR, New Delhi for a senior research fellowship.

References

[1] Industrial Organic Chemical, Ullmann's Encyclopedia, vol. 1, Wiley–VCH, 1999, p. 507.
[2] F.M. Bautista, J.M. Campelo, G.D. Luna, J.M. Marinas, A.A. Romero, M.R. Urbano, J. Catal. 172 (1997) 103.
[3] I. Ivanova, E. Pomakhina, A. Rebrov, M. Hunger, Y. Kolyagin, J. Weitkamp, J. Catal. 203 (2001) 375.
[4] L.J. Garces, V.D. Makwana, B. Hincapie, A. Sacco, S.L. Suib, J. Catal. 217 (2003) 107.
[5] F.M. Bautista, J.M. Campelo, G.D. Luna, J.M. Marinas, A.A. Romero, Appl. Catal. A 166 (1998) 39.
[6] S. Narayanan, K. Deshpande, Appl. Catal. A 199 (2000) 1.
[7] A.K. Bhattacharya, S.K. Nandi, Ind. Eng. Chem. Prod. Res. Dev. 14 (1975) 162.
[8] L.K. Doraiswamy, G.R.W. Krishnan, S.P. Mukherjee, Chem. Eng. 88 (1981) 78.
[9] M. Onaka, A. Umezono, M. Kawai, Y. Izumi, J. Chem. Soc. Chem. Comm. (1985) 1202.
[10] H. Matsuhashi, K. Arata, Bull. Chem. Soc. Jpn. 64 (1991) 2605.
[11] J. Santhalakshmi, T. Raja, Appl. Catal. A 147 (1996) 69.
[12] A.K. Ko, C.L. Young, W.D. Zhu, H.E. Lin, Appl. Catal. A 134 (1996) 53.
[13] S. Narayanan, V. Durgakumari, A.S. Rao, Appl. Catal. A 111 (1994) 133.
[14] B.L. Su, D. Barthomeuf, Appl. Catal. A 124 (1995) 73.
[15] B.L. Su, D. Barthomeuf, Appl. Catal. A 124 (1995) 81.
[16] P.S. Singh, R. Bandyopadhyay, B.S. Rao, Appl. Catal. A 136 (1996) 177.
[17] S. Prasad, B.S. Rao, J. Mol. Catal. 62 (2) (1990) L17.
[18] F.M. Baustista, J.M. Campelo, G.D. Luna, J.M. Marinas, A.A. Romero, Stud. Surf. Sci. Catal. 108 (1997) 123.
[19] S.P. Elangovan, C. Kannan, B. Arabindo, V. Murugesan, Appl. Catal. A 174 (1998) 213.
[20] P.R. Hariparasad Rao, P. Massiani, D. Barthomeuf, Catal. Lett. 31 (1995) 115.
[21] (a) T. Mathew, N.R. Shiju, K. Sreekumar, B.S. Rao, C.S. Gopinath, J. Catal. 210 (2002) 405;
(b) T. Mathew, B.B. Tope, N.R. Shiju, S.G. Hegde, B.S. Rao, C.S. Gopinath, Phys. Chem. Chem. Phys. 4 (2002) 4260.
[22] T. Mathew, M. Vijayaraj, S. Pai, B.B. Tope, B.S. Rao, S.G. Hegde, C.S. Gopinath, J. Catal. 227 (2004) 175.
[23] T. Mathew, S. Shylesh, B.M. Devassy, M. Vijayaraj, C.V.V. Satyanarayana, B.S. Rao, C.S. Gopinath, Appl. Catal. A 273 (2004) 35.
[24] T. Mathew, B.S. Rao, C.S. Gopinath, J. Catal. 222 (2004) 107.
[25] M. Vijayaraj, C.S. Gopinath, J. Catal. 226 (2004) 230.
[26] M. Vijayaraj, B. Murugan, S.B. Umbarkar, S.G. Hegde, C.S. Gopinath, J. Mol. Catal. A 231 (2005) 169.
[27] T. Mathew, N.R. Shiju, V.V. Bokade, B.S. Rao, C.S. Gopinath, Catal. Lett. 94 (2004) 223.
[28] N.F.M. Henry, J. Lipson, W.A. Wooster, The Interpretation of X-Ray Diffraction Photographs, Macmillan, London, 1951.
[29] V.L.J. Joly, P.A. Joy, S.K. Date, C.S. Gopinath, Phys. Rev. B 65 (2002) 184416.
[30] C.S. Gopinath, S. Subramanian, M. Paranthaman, A.M. Herman, Phys. Rev. B 48 (1993) 15999.
[31] C.S. Gopinath, S. Subramanian, P.S. Prabhu, M.S.R. Rao, G.V.S. Rao, Physica C 218 (1993) 117.
[32] S. Velu, K. Suzuki, H. Yoshida, T. Hattori, Phys. Chem. Chem. Phys. 4 (2002) 1990.
[33] S. Velu, K. Suzuki, C.S. Gopinath, J. Phys. Chem. B 106 (2002) 12737.
[34] S. Velu, K. Suzuki, M. Vijayaraj, S. Barman, C.S. Gopinath, Appl. Catal. B 55 (2004) 281.
[35] G. Moretti, G. Fierro, M.L. Jacono, P. Porta, Surf. Interface Anal. 14 (1989) 325.
[36] P. Mills, J.L. Sullivan, J. Phys. D 16 (1983) 723.
[37] T. Fujil, F.M.F. deGroot, G.A. Sawatzky, F.C. Voogt, T. Hibma, K. Okada, Phys. Rev. B 59 (1999) 3295.
[38] J.J. Yeh, I. Lindau, Atom. Data Nucl. Data Tables 32 (1985) 1.
[39] T. Kotanigawa, M. Yamamoto, K. Shimokawa, Y. Yoshida, Bull. Chem. Soc. Jpn. 44 (1971) 1961.
[40] S.M. Mascaros, R.M. Navarro, L.G. Sainero, U. Costantio, M. Nocchetti, L.G. Fierro, J. Catal. 198 (2001) 338.
[41] Moretti, J. Electron Spectrosc. Relat. Phenom. 76 (1995) 365.
[42] S. Poulston, P.M. Parlett, P. Stone, M. Bowker, Surf. Interface Anal. 24 (1996) 811.
[43] S. Velu, K. Suzuki, M. Okazaki, M.P. Kapoor, T. Osaki, F. Ohashi, J. Catal. 194 (2000) 373.
[44] S. Murcia-Mascaros, R.M. Navarro, L. Gomez-Sainero, U. Costantino, M. Nocchetti, J.L.G. Fierro, J. Catal. 198 (2001) 338.
[45] M. Turco, G. Bagnasco, U. Costantino, F. Marmottini, T. Montanari, G. Ramis, G. Busca, J. Catal. 228 (2004) 43, and references there in.